Identification of a Specific Inhibitor of the Dishevelled PDZ Domain†

Jufang Shan,‡ De-Li Shi,§ Junmei Wang,|| and Jie Zheng*,‡

Department of Structural Biology, St. Jude Children's Research Hospital, Memphis, Tennessee 38105, Department of Molecular Sciences and Interdisciplinary Program, University of Tennessee, Memphis, Tennessee 38163, Laboratoire de Biologie du Développement, CNRS UMR 7622, University Pierre et Marie Curie, 9 Quai Saint-Bernard, 75005 Paris, France, and Chemistry & Biophysics, Encysive Pharmaceuticals Inc., Houston, Texas 77030

Received June 30, 2005; Revised Manuscript Received September 27, 2005

ABSTRACT: The Wnt signaling pathways are involved in embryo development as well as in tumorigenesis. Dishevelled (Dvl) transduces Wnt signals from the receptor Frizzled (Fz) to downstream components in canonical and noncanonical Wnt signaling pathways. The Dvl PDZ domain is thought to play an essential role in both pathways, and we recently demonstrated that the Dvl PDZ domain binds directly to Fz receptors. In this study, using structure-based virtual ligand screening, we identified an organic molecule (NSC668036) from the National Cancer Institute small-molecule library that can bind to the Dvl PDZ domain. We then used molecular dynamics simulation to analyze the binding between the PDZ domain and NSC668036 in detail. In addition, we showed that, in *Xenopus*, as expected, NSC668036 inhibited the signaling induced by Wnt3A. This compound provides a basis for rational design of high-affinity inhibitors of the PDZ domain, which can block Wnt signaling by interrupting the Fz−Dvl interaction.

Wnt signaling pathways play important roles in embryonic and postembryonic development and have been implicated in tumorigenesis (*1*−*3*). In the canonical Wnt−β-catenin pathway, secreted Wnt glycoproteins bind to seven-transmembrane Frizzled (Fz)[1] receptors and activate intracellular Dishevelled (Dvl) proteins. Activated Dvl proteins then inhibit glycogen synthase kinase-3β (GSK-3β); this inhibition causes destabilization of a molecular complex formed by GSK-3β, adenomatous polyposis coli (APC), axin, and β-catenin and weakens the ability of GSK-3β to phosphorylate β-catenin. Unphosphorylated β-catenin proteins escape from ubiquination and degradation and accumulate in the cytoplasm. This accumulation leads to the translocation of β-catenin into the nucleus, where it stimulates transcription of Wnt target genes, such as *Myc* and the gene encoding cyclin D. Numerous reports address mutations of Wnt−β-catenin signaling pathway components that are involved in the development of neoplasia (*2*, *3*).

The link between the Wnt pathway and cancer dates back to the initial discovery of Wnt signaling: the first vertebrate Wnt growth factor was identified as the product of a cellular oncogene (*wnt-1*), which is activated by proviral insertion in murine mammary carcinomas (*4*, *5*). Perhaps the most compelling evidence supporting the role of Wnt signaling in oncogenesis is the finding that approximately 85% of colorectal cancers are characterized by mutations in APC, one of the key components of the Wnt pathway (*6*). Members of the Wnt signaling pathway also have been implicated in the pathogenesis of various pediatric cancers such as Burkitt lymphoma, medulloblastoma, Wilms tumor, and neuroblastoma (*7*−*12*). Furthermore, aberrant Wnt signaling is involved in other diseases, such as osteoporosis and diabetes (*13*).

Dvl relays the Wnt signals from membrane-bound receptors to downstream components and thereby plays an essential role in the Wnt signaling pathway. Dvl proteins are highly conserved throughout the animal kingdom (*14*, *15*). Three Dvl homologues, Dvl-1−3, have been identified in mammalian systems (*16*, *17*). All three human *Dvl* genes are widely expressed in fetal and adult tissues, including brain, lung, kidney, skeletal muscle, and heart. The DVL proteins are composed of an N-terminal DIX domain, a central PDZ motif, and a C-terminal DEP domain (*18*). Of these three, the PDZ domain appears to play an important role in both the canonical and noncanonical Wnt pathways (*19*). Indeed, the PDZ domain of Dvl may be involved not only in distinguishing roles between the two pathways (*20*, *21*) but also in nuclear localization (*22*). Recently, we investigated the interactions between the PDZ domain (residues 247−341) of mouse Dvl-1 (mDvl1) and its binding partners by using nuclear magnetic resonance (NMR) spectroscopy. We showed that the peptide-interacting site of the mDvl1 PDZ domain interacts with various molecules whose sequences have no obvious homology (*23*). Although it is not a typical PDZ-binding motif (*24*), one peptide that

† This work is supported by a Cancer Center Support Grant (CA21765) from the National Cancer Institute, by the American Lebanese Syrian Associated Charities, by Grant GM061739 from the National Institutes of Health (to J.Z.), and by the Centre National de la Recherche Scientifique and the Association pour la Recherche sur le Cancer LNCC and ARC (to D.-L.S.).

* To whom correspondence should be addressed. Telephone: (901) 495-3168. Fax: (901) 495-3032. E-mail: jie.zheng@stjude.org.

‡ St. Jude Children's Research Hospital and University of Tennessee.

§ University Pierre et Marie Curie.

|| Encysive Pharmaceuticals Inc.

[1] Abbreviations: Dvl, Dishevelled; Fz, Frizzled; PDZ, Post Synaptic Density-95, discs-large, and Zonula occludens-1; NMR, nuclear magnetic resonance; mDvl1, mouse Dishevelled 1; TMR, 2-{[5(6)-tetramethylrhodamine]carboxylamino}ethyl methanethiosulfonate; HSQC, heteronuclear single-quantum correlation; MD, molecular dynamics; rmsd, root-mean-square deviation; ODC, ornithine decarboxylase.

10.1021/bi0512602 CCC: $30.25
Published on Web 11/05/2005

binds to the mDvl1 PDZ domain is the conserved motif (KTXXXW) of Fz, which begins two amino acids after the seventh transmembrane domain (*25*). This finding showed that there is a direct interaction between Fz and Dvl and revealed a previously unknown connection between the membrane-bound receptor and downstream components of the Wnt signaling pathways. Therefore, an inhibitor of the Dvl PDZ domain is likely to effectively block the Wnt signaling pathway at the Dvl level.

The special role of the Dvl PDZ domain in the Wnt−β-catenin pathway makes it an ideal pharmaceutical target. Small organic inhibitors of the PDZ domain in Dvl might be useful in dissecting molecular mechanisms and formulating pharmaceutical agents that target cancers or other diseases in which Wnt signaling is involved. Because the structure of the Dvl PDZ domain is known, this has permitted us to use structure-based virtual ligand screening to computationally access potential ligands, leading to identification of an organic compound, NSC668036, which binds to the Dvl PDZ domain. Further NMR experiments confirmed that the compound binds to the peptide-binding site on the surface of the PDZ domain; the binding affinity (dissociation constant, K_D) of the compound was measured by fluorescence spectroscopy. In addition, we carried out molecular dynamics (MD) simulations of the interaction between this compound and the PDZ domain as well as that between the C-terminal region of a known PDZ domain inhibitor (Dapper) and the PDZ domain, and we compared the binding free energies of these interactions calculated via the molecular mechanics Poisson−Boltzmann surface area (MM-PBSA) method (*26*−*28*). Finally, we carried out a series of *in vivo* studies and demonstrated that *in Xenopus*, as expected, NSC668036 inhibited the Wnt signaling induced by Wnt3A but not by β-catenin, which is downstream of Dvl.

EXPERIMENTAL PROCEDURES

Purification of the ^{15}N-Labeled mDvl1 PDZ Domain. The ^{15}N-labeled mouse Dvl1 PDZ domain (residues 247−341 of mDvl1) was prepared as described previously (*23*, *29*). To increase the solubility of the protein, Cys338, which is located outside the ligand binding site, was mutated to alanine in the PDZ domain construct (*23*).

Preparation of the 2-{[5(6)-Tetramethylrhodamine]-carboxylamino}ethyl Methanethiosulfonate (TMR)-Linked mDvl1 PDZ Domain. Wild-type PDZ domain protein (without the Cys338Ala mutation) was produced using the standard procedure (*23*, *29*). Cys338 is the only cysteine in the protein. Purified PDZ (40 μM) was dialyzed against 100 mM potassium phosphate buffer (pH 7.5) at 4 °C overnight to remove DTT, which was added during protein purification steps to prevent disulfide bond formation. We then added dropwise a 10-fold molar excess of TMR dissolved in DMSO to the solution of the PDZ domain while it was kept stirring. After reaction for 2 h at room temperature, excess TMR and other reactants were removed by extensive dialysis against 100 mM potassium phosphate buffer (pH 7.5) at 4 °C. To assess whether the ligated TMR affects the structure of PDZ domain, we carried out the ^{15}N HSQC experiment with the TMR−PDZ sample. The ^{15}N HSQC spectrum of the TMR−PDZ sample was not significantly different from the spectrum of PDZ, indicating that PDZ had little conformational change upon the attachment of TMR. Furthermore, when the Dapper peptide was titrated into the solution of the TMR−PDZ form, significant chemical shift perturbations were observed. Those chemical shift perturbations were similar to that when the Dapper peptide was titrated into the solution of the PDZ domain, suggesting that the ligand binding capacity of the PDZ domain is preserved upon linkage of the fluorophore.

Structure-Based Ligand Screening of Small Compounds Binding to the PDZ Domain. We used the UNITY module of the SYBYL software package (Tripos, Inc.) to screen the NCI small-molecule three-dimensional database for chemical compounds that could fit into the peptide-binding groove of the Dvl PDZ domain [PDB entry 1L6O (*30*)]. The candidate compounds then were docked into the binding groove by using the FlexX module of SYBYL (Tripos, Inc.) (*31*). The compounds that exhibited the highest consensus binding scores were acquired from the Drug Synthesis and Chemistry Branch, Developmental Therapeutics Program, Division of Cancer Treatment and Diagnosis, National Cancer Institute (http://129.43.27.140/ncidb2/), for further tests.

NMR Spectroscopy. NMR ^{15}N HSQC experiments were performed by using a Varian Inova 600 MHz NMR spectrometer at 25 °C. Samples consisted of the Dvl PDZ domain (0.3 mM) in 100 mM potassium phosphate buffer (pH 7.5), 10% D_2O, and 0.5 mM EDTA. NMR spectra were processed with NMRpipe (*32*) and analyzed by using Sparky (*33*).

Fluorescence Spectroscopy. We used a Fluorolog-3 spectrofluorometer (Jobin-Yvon, Inc.) to obtain the fluorescence measurements of the interaction between the TMR-linked PDZ domain and the NSC668036 compound. Titration experiments were performed at 25 °C in 100 mM potassium phosphate buffer (pH 7.5). The stock solution of ligand was sequentially injected into a fluorescence sample cell that contained 2 mL of 40 nM TMR-labeled PDZ domain in 100 mM potassium phosphate buffer (pH 7.5). The concentration of the stock solution of NSC668036 is 1 mM. During the fluorescence measurement, the excitation wavelength was 552 nm, and the emission wavelength was 579 nm. The fluorescence data were analyzed by using ORIGIN (Microcal Software, Inc.). The equation $1/\Delta F = a(1/[S]) + b$ was used to fit the double-reciprocal plot of the fluorescence data, where ΔF is the change in the fluorescence intensity and [S] is the ligand concentration. The K_D was calculated from the fitted values of a and b ($K_D = a/b$).

Molecular Dynamics Simulation. MD simulation was performed by using the sander program in AMBER 8 with the parm99 force field (*34*, *35*). AM1-BCC charges were assigned to NSC668036 by using the Antechamber module (*36*) in AMBER 8. The starting structures of ligand−protein complexes were prepared using the output from the FlexX docking studies. After neutralization, complexes were dissolved in a periodic rectangular TIP3P water box, with each side 10 Å from the edge of the complex. The components of these MD systems are summarized in Table S1 of the Supporting Information. Systems were minimized by a 1000-step steepest descent minimization followed by a 9000-step conjugated gradient minimization (*34*, *35*). The MD simulations were performed with a time step of 2 fs and the nonbonded cutoff set to 9.0 Å. Constant volume (NVT) and constant pressure (NPT) ensemble simulations were carried out to equilibrate the system. In detail, a 50 ps NVT

simulation was used to increase the temperature from 100 to 300 K; then the 50 ps NPT ensemble was used to adjust the solvent density, and another 100 ps NPT ensemble was used to gradually reduce the harmonic restraints from 5.0 kcal mol^{-1} Å^{-2} to none (*34*, *35*). A 5 ns MD production run was then carried out using the NPT ensemble. During the production run, snapshots were saved every 5 ps. Other simulation parameters were set to values similar to those described in the work by Gohlke et al. (*37*).

Binding Free Energy Calculation. The binding free energy was calculated using eq 1 by the mm_pbsa.pl script in AMBER 8, which employs an MM-PBSA approach.

$$\Delta G_{\text{total}} = G^{\text{complex}} - G^{\text{protein}} - G^{\text{ligand}} \quad (1)$$

where

$$G = H_{\text{gas}} + H_{\text{trans/rot}} + G_{\text{solvation}} - TS \quad (2)$$

$$G_{\text{solvation}} = G^{\text{polar}}_{\text{solvation}} + G^{\text{nonpolar}}_{\text{solvation}} \quad (3)$$

$$G^{\text{nonpolar}}_{\text{solvation}} = \gamma A + b \quad (4)$$

where the gas phase energy, H_{gas}, is the sum of internal (bond, angle, and torsion), van der Waals, and electrostatic energies in the molecular mechanical force field with no cutoff, as calculated by molecular mechanics (*38*). $H_{\text{trans/rot}}$ is 3*RT* (*R* being the gas constant) because of six translational and rotational degrees of freedom. The solvation free energy, $G_{\text{solvation}}$, was calculated by using the PB model (*26*, *37*, *38*). In PB calculations, the polar solvation energy, $G^{\text{polar}}_{\text{solvation}}$, was obtained by solving the PB equation with Delphi using parse radius, parm94 charges (for the PDZ domain and the Dapper peptide), and AM1-BCC charges (for the compound). The nonpolar contribution was calculated by eq 4. In this equation, *A* is the solvent accessible area calculated by the Molsurf module in Amber 8 and γ (surface tension) and *b* (a constant) were 0.00542 kcal mol^{-1} Å^{-2} and 0.92 kcal mol^{-1}, respectively. All of the energy terms given above were averaged from 150 snapshots extracted every 20 ps, and the entropy *TS* was estimated by normal-mode analysis using 15 snapshots extracted every 200 ps during the last 3 ns production run.

Xenopus Embryos and Microinjections of mRNA and Peptides. Xenopus eggs were obtained from females that had received injections of 500 IU of human chorionic gonadotropin (Sigma) and had been artificially fertilized. Synthesis and microinjection of capped mRNAs were carried out as described previously (*23*, *25*). To assess secondary axis formation, the mRNAs and compound NSC668036 were injected into the ventro-vegetal blastomere of four-cell embryos, and the embryos were then cultured until they reached the larval stage.

RT-PCR. The mRNAs and compound NSC668036 were injected into the animal pole region of *Xenopus* embryos at the two-cell stage. Animal cap explants from control and treated embryos at the blastula stage were dissected and then cultured until they reached the early gastrula stage. Extraction of RNA, RT-PCR, and primers for Siamois and ODC were as described previously (*23*, *25*). The RT-PCR results were analyzed by using a phosphoimager system (Bio-Rad).

RESULTS

Structure-Based Ligand Screening. We searched for potential inhibitors of the PDZ domain of Dvl binding to Fz using structure-based virtual screening. PDZ is a modular protein interaction domain that has two α helices and six β sheets (*39*). The αB helix and βB sheet together with the loop that precedes them form a peptide-binding cleft. In their crystal complex structure, the Dapper peptide (derived from one of the binding partners of the Dvl PDZ domain) forms hydrogen bonds with residues Leu265, Gly266, Ile267, and Ile269 in the βB sheet of the PDZ domain (*30*).

To identify small organic compounds that can bind to this groove and interrupt interactions between the PDZ domain and its binding partners, we first designed a query by using UNITY, a module in SYBYL (Tripos, Inc.). The query consisted of two hydrogen bond donors (backbone amide nitrogens of Gly266 and Ile269) and two hydrogen bond acceptors (carbonyl oxygens of Ile267 and Ile269) on the PDZ domain, with 0.3 Å tolerances for spatial constraints. We then used the Flex search module of UNITY to explore the three-dimensional (3D) small-molecule database of the National Cancer Institute (NCI) to identify compounds that met the requirements of the query. The 3D database is available from NCI at no cost, and it includes the coordinates of more than 250 000 druglike chemical compounds. The Flex search option of UNITY considers the flexibility of compounds, and it uses the Directed Tweak algorithm to conduct a rapid and conformationally flexible 3D search (*40*). The search we performed yielded 108 organic compounds as the initial hits.

These 108 hits then were "docked" into the binding site of the PDZ domain by using the FlexX program of SYBYL. FlexX is energy minimization modeling software that varies the conformation of the ligand to fit it into the protein-binding site (*41*). As a control, we also docked the Dapper peptide into the PDZ domain. The receptor's binding site was defined by residues Gly266, Ile269, and Arg325 with a selection radius of 5.9 Å, and a core subpocket was defined by Gly266 with a selection radius of 5.9 Å. Under this condition, the docked Dapper peptide had a conformation similar to that found in the crystal structure of the complex with a backbone root-mean-square deviation (rmsd) of 2.04 Å. In particular, the backbone rmsd for the last six C-terminal amino acids is 1.22 Å, indicating that the docking procedure we used is able to dock ligand into the binding site of the PDZ domain with reasonable accuracy. We evaluated the results of the docking procedure and manually removed those compounds that were not docked into the binding pocket of the PDZ domain. Then we used the Cscore program of SYBYL to rank the remaining compounds on the basis of their predicted ability to bind to the binding pocket. Cscore generates a relative, consensus score, based on the individual scoring functions of the protein−ligand complex (*42*). One of the scoring functions in Cscore, the *F*_score, is particularly useful. *F*_score considers polar and nonpolar interactions in calculating the binding free energy of ligand and protein. We then further characterized nine available chemicals whose *F*_scores were better than that of the control Dapper−PDZ interaction; we obtained these compounds from the Developmental Therapeutics Program (DTP) of the NCI.

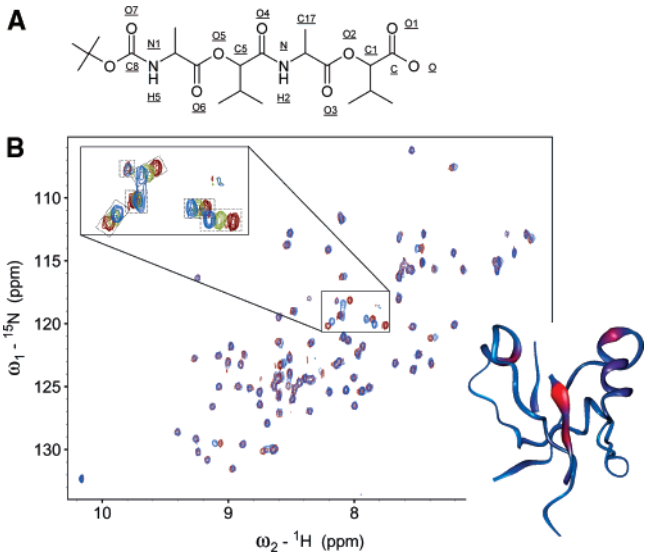

FIGURE 1: Interaction between the mDvl1 PDZ domain and NSC668036. (A) Structure of compound NSC668036. The chemical structure of NSC668036 was sketched by using ISIS/Draw (MDL Information Systems, Inc.). Some atoms (which are mentioned in the text) are labeled with the atom name assigned by the Antechamber module of AMBER 8. (B) ^{15}N HSQC spectra of free NSC668036 (red contour lines) and of NSC668036 bound to the PDZ domain of mDvl1 (blue contour lines) are shown. The concentration of the PDZ domain was 0.3 mM. The concentration of NSC668036 was 7.8 mM (bound form). In the top inset, the signals from the same region with enlarged spectra were placed in smaller boxes. The inset also contains an additional spectrum (green lines) from a different concentration of NSC668036 (2.4 mM). In the worm representation of the backbone structure of the mDvl1 PDZ domain (bottom inset), the thickness of the worm is proportional to the weighted sum (in hertz) of the ^{1}H and ^{15}N shifts upon binding by NSC668036; increasing chemical shift perturbation is shown (blue for low and red for high). This figure was prepared by using Insight II (Accelrys, Inc.). A ribbon diagram of the same PDZ domain is also shown in Figure 4A.

Binding of NSC668036 to the PDZ Domain. We tested the abilities of the nine compounds obtained from DTP to bind to the PDZ domain by using NMR spectroscopy, mainly the chemical shift perturbation experiment (*43*). Among these nine compounds, NSC668036 (MW = 461 Da; Figure 1A) generated chemical shift perturbations to the resonances of the Dvl PDZ domain when added to a solution of the ^{15}N-labeled Dvl PDZ domain (residues 247−341 of mouse Dvl1): the series of ^{1}H−^{15}N correlation spectra exhibited prominent chemical shift perturbations of Ile264, Ser265, Val289, Ala290, Arg322, and Val325 in the PDZ domain (Figure 1B). Residues Ile264 and Ser265 are in the βB sheet of the PDZ domain, whereas Arg322 and Val325 are in the αA helix. The binding site of compound NSC668036 on the mDvl1 PDZ domain can be further illustrated by a "backbone worm" representation of the PDZ domain (Figure 1B). The thickness of the worm is proportional to the weighted sum of the ^{1}H and ^{15}N chemical shift perturbations [colored from blue (low) to red (high)] induced by the binding of NSC668036. These chemical shift perturbations were similar to those caused by binding of the Dapper peptide and Fz7 peptide, which was derived from a Fz membrane receptor (*23*). This result suggests that compound NSC668036 binds to the same binding site as native PDZ domain-binding partners such as Dapper and Fz. Therefore, NSC668036 may be able to disrupt functional interactions of the PDZ domain and thereby inhibit Wnt−Fz signaling pathways.

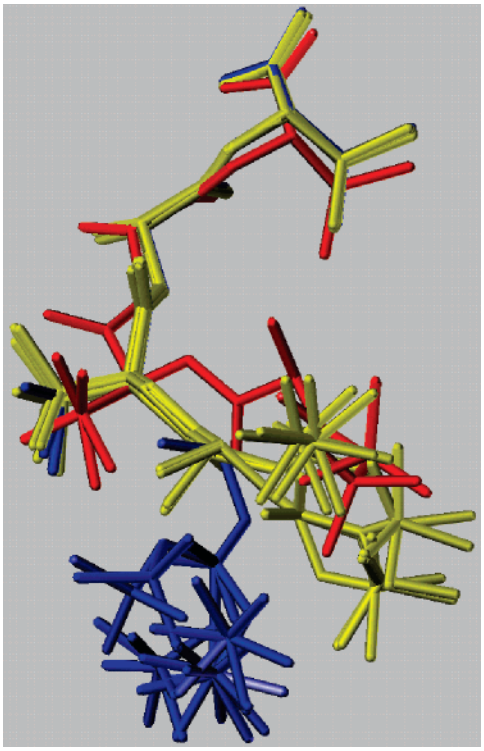

FIGURE 2: Thirty docking conformations of compound NSC668036 generated by using FlexX were clustered into three groups. Group I comprised five conformations (red) with rmsds between 0.46 and 0.77 Å, group II 13 conformations (yellow) with rmsds between 1.44 and 1.73 Å, and group III 12 conformations (blue) with rmsds between 2.31 and 2.86 Å.

To determine the binding affinity of NSC668036, we conducted fluorescence spectroscopy experiments by using fluorophore-labeled PDZ domain (TMR−PDZ). We followed the quenching of fluorescence emission of TMR−PDZ at 579 nm (with the excitation at 552 nm) as we titrated NSC668036 into the TMR−PDZ solution. The fluorescence emission of TMR was quenched because of the binding of NSC668036 to the PDZ domain. A double-reciprocal plot of the fluorescence changes against the concentrations of NSC668036 gave a linear correlation. Linear fitting using Origin (Microcal Software, Inc.) calculated a K_D (mean ± standard deviation) of 237 ± 31 μM (Figure S1 of the Supporting Information).

Molecular Dynamics Simulations of the Complex between the Dvl PDZ Domain and NSC668036. To further investigate the interaction between the PDZ domain and NSC668036, we used the AMBER software suite to conduct a molecular dynamics (MD) simulation study of the NSC668036−PDZ domain complex. MD simulations were performed in explicit water for 5 ns after equilibration with the particle mesh Ewald (PME) method (*44*, *45*). We then used the MM-PBSA algorithm (*26*−*28*) to calculate the binding free energy of the interaction between the PDZ domain and NSC668036.

To sample sufficient possible binding modes during the MD simulation, we re-examined the entire output of the initial FlexX docking results. The default settings of the FlexX docking algorithm yielded 30 possible docking conformations (Figure 2), and the conformers which had the best docking scores were selected. Although the conforma-

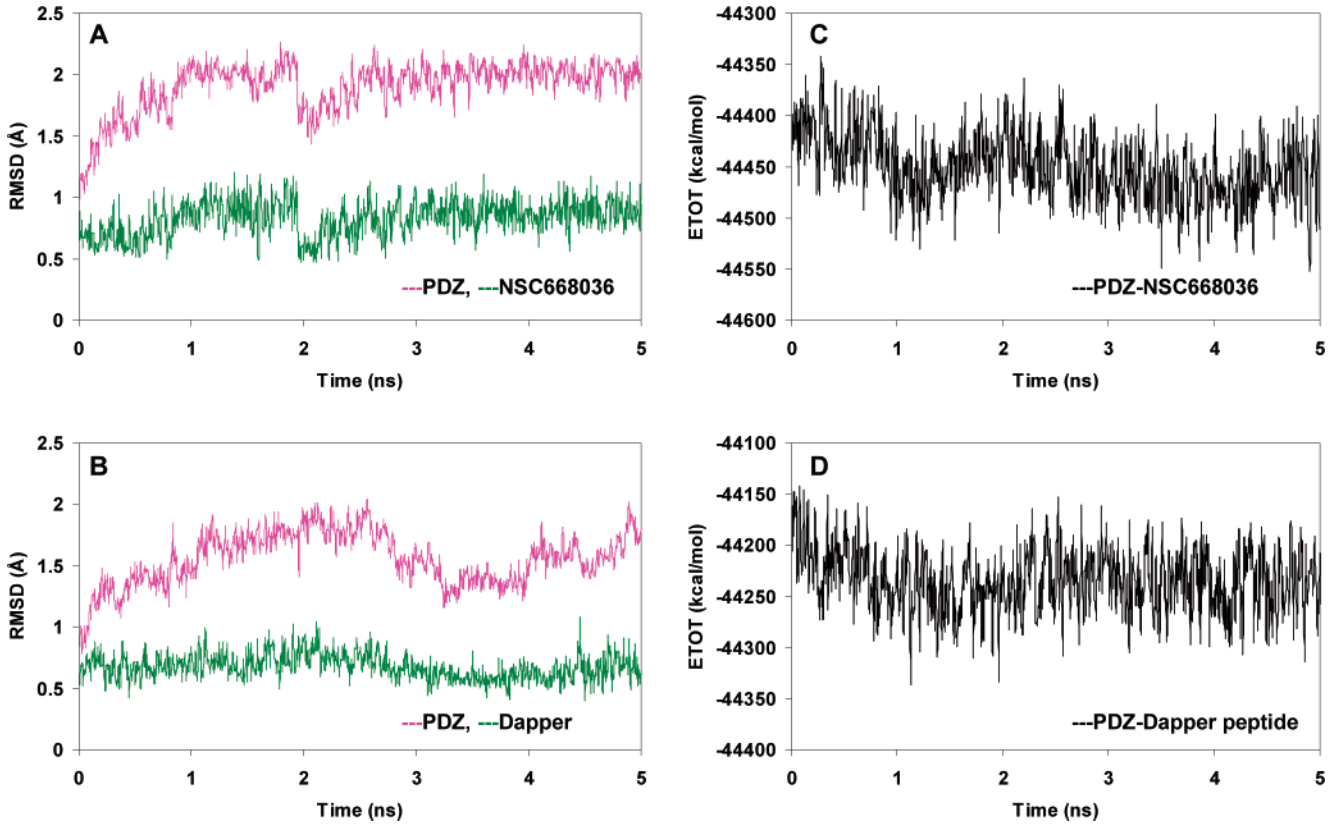

FIGURE 3: Backbone root-mean-square deviations (rmsds, Å) of the mDvl1 PDZ domain bound to NSC668036 and of the mDvl1 PDZ domain bound to the Dapper peptide vs the starting structure and total potential energies of the MD systems for 5 ns explicit simulations. (A) Backbone rmsds of the mDvl1 PDZ domain (magenta) and NSC668036 (green) for a 5 ns simulation. (B) Backbone rmsds of the Dvl1 PDZ domain (magenta) and Dapper peptide (green) for a 5 ns simulation. (C) The total potential energy (ETOT) of the mDvl1 PDZ domain and NSC668036 (water molecules included) during a 5 ns simulation fluctuated between −44552.6 and −44344.2 kcal/mol. The total potential energy (mean ± standard deviation) was −44450.8 ± 32.6 kcal/mol. (D) The total potential energy of the Dvl1 PDZ domain (water molecules included) and Dapper peptide during a 5 ns simulation fluctuated between −44349.8 and −44122.3 kcal/mol. The total potential energy (mean ± standard deviation) was −44233.8 ± 31.3 kcal/mol. The 200 ps equilibration phase is not included.

tions of the 30 docked NSC668036 conformers were very similar overall, there were distinct variations. These 30 bound conformers can be clustered into three main groups. Group I comprises five conformers, and the rmsds of all the atoms in NSC668036 are between 0.46 and 0.77 Å for this group of conformers; group II has 13 conformers with rmsds between 1.44 and 1.7 Å, and group III has 12 conformers with rmsds between 2.31 and 2.86 Å (Figure 2). Manual inspection of these docking conformers led us to select 10 conformers as starting points for the MD simulations (see Table S1 for the components of the MD systems). Of these 10 conformers, one was from group I (conformer 6), five were from group II (conformers 4, 7, 10, 14, and 15), and four were from group III (conformers 12, 22, 26, and 27). During the 10 MD simulation runs, the simulation that started with conformer 22 (group III) had the lowest and most stable binding free energy, suggesting that this conformer represents the true PDZ domain-bound conformation of NSC668036 in solution.

Structure of the NSC668036-Bound Dvl PDZ Domain. We analyzed the MD simulation that started with conformer 22 in detail. During the 5 ns MD production run, the total energy of the MD system (water box included) fluctuated between −44552.6 and −44344.2 kcal/mol (mean of −44450.8 kcal/mol) with a root-mean-square deviation (rmsd) of 32.6 kcal/mol (Figure 3A,C). The lowest energy occurs at 4.905 ns; the structure of mDvl1 bound with NSC668036 at this point is shown in Figure 4B. In the complex, NSC668036 formed hydrogen bonds with residues Leu262, Gly263, Ile264, Ile266, and Arg322 of the Dvl PDZ domain (Figure 4B); close hydrophobic contacts between the ligand and the residues in the PDZ domain were also observed. For example, the valyl group that is connected to C1 was within 3.5 Å of the hydrophobic side chains of residues Leu262, Ile264, Ile266, Leu321, and Val318 as well as the C_α side chain of Arg322. In addition, the C17 methyl group was within 3.5 Å of Phe261, and the "C"-terminal *tert*-butyl group had hydrophobic contacts with Val267 and Val318 (within 3.5 Å of the hydrophobic side chains of the two residues).

Bound NSC668036 Adopts a Conformation Similar to, but Not Exactly the Same as, That of the Bound Dapper Peptide. A comparison between the crystal structure of the PDZ domain bound with the Dapper peptide (*30*) and the simulated NSC668036−PDZ domain complex revealed that both ligands adopt similar conformations when bound to the PDZ domain (Figure 4). The mass-weighted backbone rmsd (only the four C-terminal amino acids, MTTV, were included in the rmsd calculation) for both the PDZ domain-bound NSC668036 and the PDZ domain-bound Dapper peptide was 1.49 Å. The backbone of NSC668036 was defined as the atoms in the main chain between and including the carbonyl carbon of the carboxylate group (C) and the carbonyl carbon at the other end of NSC668036 (C8) (a total of 13 atoms; Figure 1A).

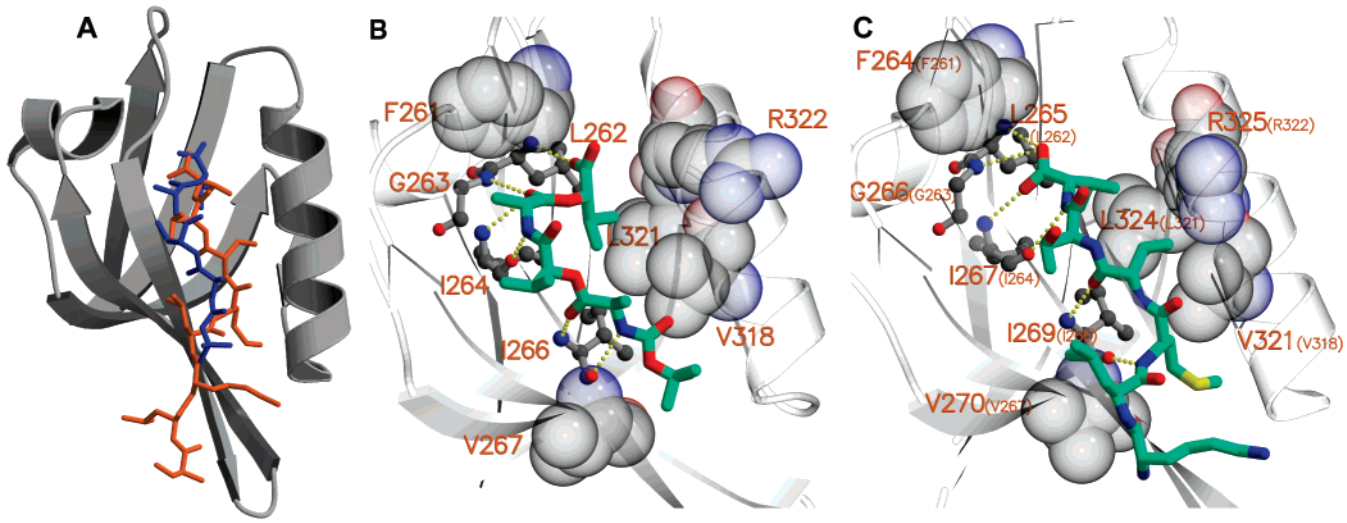

FIGURE 4: Conformation of NSC668036 docked into the PDZ domain and of the NSC668036−mDvl1 PDZ domain complex. (A) NSC668036 and the Dapper peptide bound to the PDZ domain in similar conformations. NSC668036 (blue) was docked into the Dvl PDZ domain (ribbons and tubes colored gray) by using FlexX (Tripos, Inc.). The Dapper peptide (orange) is in its conformation determined by X-ray crystallography and is in a complex with the PDZ domain. The difference between the backbone root-mean-square deviation of compound NSC668036 and that of Dapper peptide [only the backbone atoms of the four C-terminal amino acids (MTTV) were used] was 1.49 Å. (B) Binding conformation of NSC668036 at 4.905 ns during the 5 ns simulation. The PDZ domain is shown as gray ribbons and tubes. NSC668036 is represented according to the bound atom (green for carbon, red for oxygen, and blue for nitrogen). Residues that formed a hydrogen bond with the compound are shown in ball-and-stick format (black for carbon, red for oxygen, and blue for nitrogen); hydrogen bonds are represented by yellow dotted lines. Residues within 3.5 Å of isopropyl, methyl (those next to nitrogen atoms), and *tert*-butyl groups are in CPK format (gray for carbon, red for oxygen, and blue for nitrogen). In addition, Leu262, Ile264, and Ile266 were within 3.5 Å of the isopropyl group next to the carboxylate group. They are in ball-and-stick format for clarity. (C) Conformation of the Dapper peptide [only the last six C-terminal amino acids (KLMTTV) are shown] bound to the *Xenopus* Dishevelled PDZ domain (PDB entry 1L6O) (*30*). Representations are the same as in panel B. Residue numbers in parentheses correspond to those of the mDvl1 PDZ domain.

Table 1: Hydrogen Bonds Observed between NSC668036 and the PDZ Domain and between the Dapper Peptide and the PDZ Domain during a 5 ns Explicit Simulation[a]

NSC668036−PDZ			Dapper peptide−PDZ		
NSC668036	PDZ	occupancy (%)	Dapper 1	PDZ	occupancy (%)
O	Leu262 N/H	13.5	Val0 OXT	Leu262 N/H	27.7
O1	Leu262 N/H	85.1	Val0 O	Leu262 N/H	98.0
O3	Gly263 N/H	91.6	Val0 OXT	Gly263 N/H	98.4
O3	Ile264 N/H	32.6	Val0 OXT	Ile264 N/H	82.3
N/H2	Ile264 O	99.8	Val0 N/H	Ile264 O	99.1
O6	Ile266 N/H	99.5	Thr−2 O	Ile266 N/H	99.8
N1/H5	Ile266 O	65.1	Met−3 N/H	Ile266 O	99.2
O7	Arg322	11.2	Lys−5 O	Gly268 N/H	99.4
			Lys−5 N/H	Gly268 O	86.9
			Ser−7 O	Ser270 N/H	85.3

[a] The length and angle cutoffs for a H-bond are 3.5 Å and 120°, respectively.

To conduct a further detailed comparison, similar to the MD simulation conducted with the PDZ domain−NSC668036 complex, we carried out a 5 ns MD simulation for the complex that consisted of the PDZ domain and Dapper peptide. For each MD simulation, we saved 1000 "snapshots" and analyzed them in detail (Figure 3). The MD simulations allowed us to compare the hydrogen bonds within the two complexes *in detail*, and those hydrogen bonds, together with their percentage occupancies in the 1000 snapshots, are listed in Table 1. Perhaps the most striking difference between the two complexes is within the hydrogen bond network between the "carboxylate binding loop" formed by the conserved Gly-Leu-Gly-Phe motif (Phe261-Leu262-Gly263-Ile264 in the mDvl1 PDZ domain) and the C-terminal residue of the bound peptide. This hydrogen bond network is the hallmark of the structure of a C-terminal peptide complex of a PDZ domain (*24*), and in the structure of the Dapper−PDZ domain complex, the amide groups of Leu262, Gly263, and Ile264 donated hydrogen bonds to the carboxylate group of the Dapper peptide. In the NSC668036−PDZ domain complex, because of the flexibility of the ether bond, the C-terminal carboxylate group and O3 were in the cis conformation. This conformation allowed both O3 and the C-terminal carboxylate group to be involved in the "hydrogen network"; the amide groups of Gly263 and Ile264 form hydrogen bonds with O3, and the C-terminal carboxylate group of NSC668036 forms a hydrogen bond with the amide group of Leu262. Outside the carboxylate binding network, the two bound ligands had very similar hydrogen bonds and hydrophobic contacts with the host PDZ domain. Therefore, the increased binding affinity of the Dapper peptide likely is due to the extra length of the peptide: residues Lys−5, Leu−6, and Ser−7 of the bound Dapper peptide form multiple hydrogen bonds and hydrophobic contacts with the host PDZ domain.

To further compare the binding of the Dapper peptide and NSC668036 to the PDZ domain, we examine the binding free energies of the complexes. The absolute binding free energies for both systems were calculated by using the MM-PBSA approach in combination with normal-mode analysis (*26*−*28*). The binding free energy was −1.88 kcal/mol for the PDZ−NSC668036 complex and −7.48 kcal/mol for the PDZ−Dapper peptide complex (see Tables 2S−4S for all the energy elements obtained from the MM-PBSA free binding energy calculations). The relative ranking of binding free energies was consistent with experimental data. Indeed, as the dissociation constants for NSC668036 and the Dapper peptide were 237 and 16 μM (*23*), respectively, at 25 °C, the binding free energies ($\Delta G = RT \ln K_D$) were −4.94 kcal/

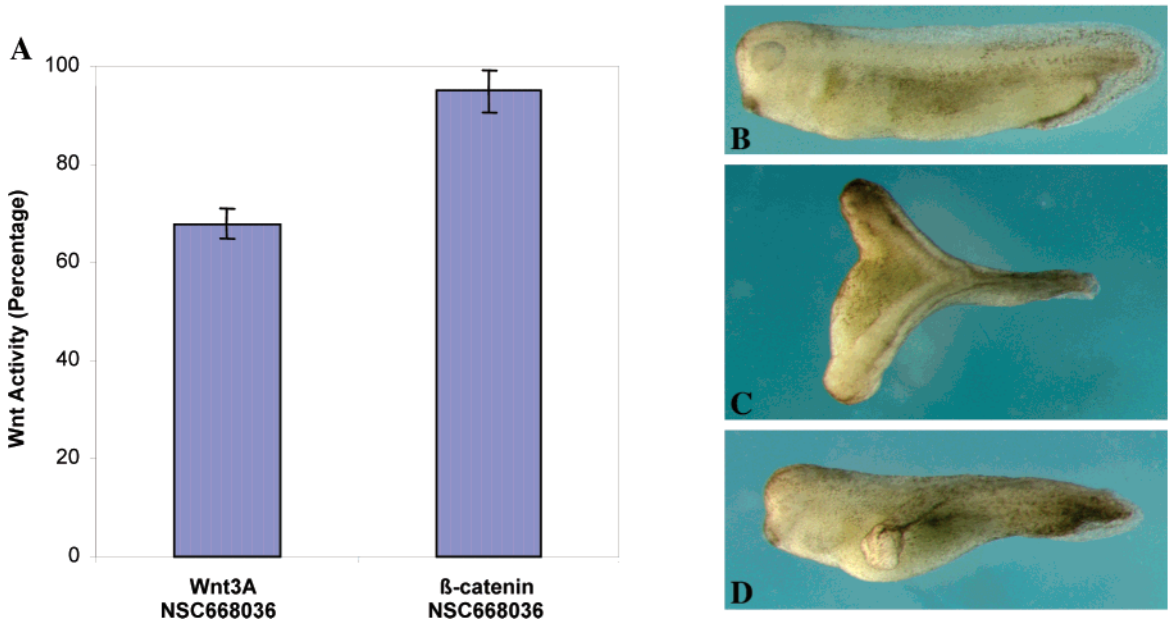

FIGURE 5: Effect of NSC668036 on canonical Wnt signaling in *Xenopus* embryos. (A) NSC668036 inhibited the canonical Wnt pathway induced by Wnt3A but not by β-catenin. RT-PCR was conducted to analyze the expression of the *Xenopus* Wnt target gene *Siamois* in ectodermal explants. Synthetic mRNAs corresponding to Wnt3A (1 pg) and β-catenin (500 pg) were injected alone or with NSC668036 (180 ng) into the animal-pole region at the two-cell stage, and ectodermal explants were cultured until they reached the early gastrula stage, at which time they underwent RT-PCR analysis. The data are a summary of two independent experiments. The activities of controls (without inhibitors) were 100%. (B) Control embryo that received no injection. (C) An embryo that received an injection of Wnt3A mRNA developed a complete secondary axis. (D) An embryo that received co-injections of Wnt3A mRNA and NSC668036 developed a partial secondary axis.

Table 2: Effect of NSC668036 on Formation of the Secondary Axis Induced by Wnt3A and β-Catenin[a]

	double axis[b]	single axis	total[c]
no injection		100%	83
Wnt3A	77%	23%	75
Wnt3A/NSC668036	55%	45%	78
β-catenin	51%	49%	78
β-catenin/NSC668036	49%	51%	76

[a] Ventro-vegetal injection of Wnt3A mRNA and β-catenin and of Wnt3A mRNA and NSC668036 at the two-cell stage. Experimental details are given in Figure 5B−D. [b] Defined as the appearance of a second neural plate on the ventral side of early neurulae and ectopic eyes and cement glands. Percentages indicate the proportion of embryos that met the definition. [c] Total number of embryos that received injections in two independent experiments.

mol for NSC668036 and −6.54 kcal/mol for the Dapper peptide.

Inhibition of the Wnt Signaling Pathway by NSC668036. In an earlier study (*23*, *25*), we demonstrated that the PDZ domain of Dvl interacts directly with the conserved sequence that is C-terminal to the seventh transmembrane helix of the Wnt receptor Fz. This interaction is essential in transduction of the Wnt signal from Fz to the downstream component of Dvl. Therefore, an inhibitor of the Dvl PDZ domain should modulate Wnt signaling by acting as an antagonist. To test whether NSC668036 can indeed inhibit Wnt signaling pathways, we co-injected NSC668036 with various activators of the canonical Wnt pathway into the animal-pole region of *Xenopus* embryos at the two-cell stage (*23*, *25*). We then performed RT-PCR to analyze expression of the Wnt target gene *Siamois* in ectodermal explants that were dissected from blastulae and cultured until their development reached the early gastrula stage. In the RT-PCR experiments, expression of ornithine decarboxylase (ODC) was used as the loading control. Although NSC668036 had little effect on *Siamois* expression induced by β-catenin, a component of Wnt signaling that is downstream of Dvl, NSC668036 inhibited *Siamois* expression induced by Wnt3A (Figure 5A). These results are consistent with the notion that binding of NSC668036 to the PDZ domain of Dvl blocks signaling in the canonical Wnt pathway at the Dvl level.

We then tested whether NSC668036 affected the well-known ability of Wnt to induce secondary axis formation (*46*). Wnt3A injected into the ventro-vegetal region of a *Xenopus* ectodermal explant induced the formation of a complete secondary axis (*46*) (Figure 5C). However, when co-injected with Wnt3A, NSC668036 substantially reduced the level of secondary axis formation induced by Wnt3A (Figure 5D). This reduction resulted in embryos with a partial secondary axis or only a single axis (Table 2). Therefore, we concluded that NSC668036 seems to specifically block signaling in the canonical Wnt pathway.

DISCUSSION

Our discovery shows that structure-based virtual ligand screening is a feasible approach to identifying small molecules that, on the basis of the structural features of the targeted protein, bind to the target. To build the search query for the virtual screening stage, in our studies, we used the crystal structure of the PDZ domain of *Xenopus* Dvl bound with the Dapper peptide (*30*) instead of the NMR solution structure of the apo-PDZ domain of mouse Dvl (*23*). The two PDZ domains share a high degree of homology, especially around the peptide-binding sites; near the binding sites, there is only a single amino acid difference between the two PDZ domains (Glu323 in the PDZ domain of mDvl1 vs Asp326 in the PDZ domain of *Xenopus* Dvl), and the side chain of this residue points away from the peptide-

binding cleft. The peptide-binding cavity of the domain is smaller in the apo form of the solution structure than in the crystal structure of the Dapper-bound PDZ domain of *Xenopus* Dvl. This difference is consistent with the classic "induce-and-fit" mechanism, in which, upon the binding of a peptide or a small organic molecule, the binding sites in the PDZ domain undergo conformational change to accommodate the bound ligand. However, this flexibility cannot be fully explored through a UNITY search and the FlexX docking protocols. Therefore, although the PDZ domain of mouse Dvl was used in the experimental studies, the crystal structure of the PDZ domain of *Xenopus* Dvl provides a better template for the virtual screening steps. Indeed, the binding free energies calculated from MD simulation of the PDZ domain−NSC668036 and PDZ domain−Dapper peptide complexes fit well with the experimental binding data.

By using a UNITY search for compounds with the potential to bind to the PDZ domain, FlexX docking of candidates into the binding site, Cscore ranking of binding modes, and chemical shift perturbation NMR experiments, we identified a small organic molecule (NSC668036) that can bind to the mDvl1 PDZ domain. NSC668036 is a peptide mimetic in which two peptide bonds are substituted with two ether bonds. Therefore, NSC668036 is expected to be more resistant to proteases *in vivo*. In addition, NSC668036 is very stable and highly soluble. Furthermore, the simple structure of NSC668036 provides an opportunity as a template for further optimizations. For example, the binding affinity is expected to increase if the branching of a hydrophobic group from the backbone of NSC668036 contacts the side chain of Phe261 in the PDZ domain.

NSC668036 interacts with the Dvl PDZ domain specifically. We tested two other PDZ domains: the first PDZ domain of PSD-95, PSD95a (*47*) (PDB entries 1IU0 and 1IU2), which belongs to the class I PDZ domains, and the PDZ7 domain of the glutamate receptor-interacting protein (*48*) (PDB entry 1M5Z), a member of the class II PDZ domains (Figure S2 shows the structure-based sequence alignment of different PDZ domains). NSC668036 binds to both of these PDZ domains extremely weakly (data not shown). The specificity of NSC668036 for the Dvl PDZ domain likely is due to a unique feature of the domain. The Dvl PDZ domain belongs to neither class I nor class II PDZ domains (*23*) (Figure S2). In particular, the Dvl PDZ domain has two loops: one between the first and second β-strands (the βA−βB loop) and the other between the second α helix and the last β-strand (the αB−βF loop). These two loops of the Dvl PDZ domain are longer than that in a typical PDZ domain. In the structure of a typical PDZ domain bound with a C-terminal peptide, the carboxylate group of the bound peptide is also linked through a bound water molecule to the guanidinium group of an arginine in the βA−βB loop (*49*). The side chain of the same arginine also forms a hydrogen bond with the amide ground of a glycine in the αB−βF loop. However, the Dvl PDZ domain lacks both the arginine and glycine, and the cavity that holds the bound water molecule in a typical PDZ domain is much smaller in the Dvl PDZ domain. Indeed, there is no bound water molecule in the crystal structure of the Dvl PDZ domain in a complex with the Dapper peptide (*30*). However, unlike the PDZ domain-bound Dapper peptide, when NSC668036 bound to the Dvl PDZ domain, O3 participated in two hydrogen bond connections with the carboxylate binding loop of the PDZ domain and the carboxylate group of the bound NSC668036 was pushed into the empty space and stayed in the narrow cavity. We speculate that this binding feature of NSC668036 may explain the specificity of the molecule for the Dvl PDZ domain; in other words, NSC668036 achieves its specificity using its unique binding mode. This notion is supported by results from one of our MD simulation studies. In the MD simulation run, the starting conformation of the PDZ domain−NSC668036 complex was created by superimposing NSC668036 over the bound Dapper peptide so that the carboxylate group of the compound formed all three hydrogen bonds with the host PDZ domain. After a 200 ps production run, the system was no longer stable (data not shown).

ACKNOWLEDGMENT

We thank Dr. Mingjie Zhang for providing DNA constructs encoding the first PDZ domain of PSD-95 and the seventh PDZ domain of GRIP, Dr. Ho-Jin Lee, Youming Shao, and the Protein Production Facility at St. Jude Children's Research Hospital for producing proteins, the Hartwell Center for Bioinformatics and Biotechnology at St. Jude for giving us computational time, Scott Malone for providing technical support for AMBER 8, Dr. Weixing Zhang for giving us assistance with the NMR experiments, Dr. Charles Ross for providing computer support, and Drs. Amy L. B. Frazier and Julia Cay Jones for editing the manuscript.

SUPPORTING INFORMATION AVAILABLE

Atom information for MD systems and dimensions of the water box (Table S1), binding free energies of Dapper and PDZ, and 10 conformations of NSC668036 and PDZ (Table S2), binding free energy components of NSC668036 and the PDZ domain (Table S3), binding free energy components of the Dapper peptide (Table S4), comparison of binding free energy components (Table S5), double-reciprocal plot of fluorescence intensity quenching of the PDZ domain by NSC668036 (Figure S1), and structure-based sequence alignment of PDZ domains (Figure S2). This material is available free of charge via the Internet at http://pubs.acs.org.

REFERENCES

1. Moon, R. T., Bowerman, B., Boutros, M., and Perrimon, N. (2002) The promise and perils of Wnt signaling through β-catenin, *Science 296*, 1644−1646.
2. Polakis, P. (2000) Wnt signaling and cancer, *Genes Dev. 14*, 1837−1851.
3. Wodarz, A., and Nusse, R. (1998) Mechanisms of Wnt signaling in development, *Annu. Rev. Cell Dev. Biol. 14*, 59−88.
4. Brown, J. D., and Moon, R. T. (1998) Wnt signaling: Why is everything so negative? *Curr. Opin. Cell Biol. 10*, 182−187.
5. van Ooyen, A., and Nusse, R. (1984) Structure and nucleotide sequence of the putative mammary oncogene int-1: Proviral insertions leave the protein-encoding domain intact, *Cell 39*, 233−240.
6. Potter, J. D. (1999) Colorectal cancer: Molecules and populations, *J. Natl. Cancer Inst. 91*, 916−932.
7. Giles, R. H., van Es, J. H., and Clevers, H. (2003) Caught up in a Wnt storm: Wnt signaling in cancer, *Biochim. Biophys. Acta 1653*, 1−24.
8. Koesters, R., and von Knebel, D. M. (2003) The Wnt signaling pathway in solid childhood tumors, *Cancer Lett. 198*, 123−138.

9. Koesters, R., Niggli, F., von Knebel, D. M., and Stallmach, T. (2003) Nuclear accumulation of β-catenin protein in Wilms' tumours, *J. Pathol. 199*, 68−76.
10. Koesters, R., Ridder, R., Kopp-Schneider, A., Betts, D., Adams, V., Niggli, F., Briner, J., and von Knebel, D. M. (1999) Mutational activation of the β-catenin proto-oncogene is a common event in the development of Wilms' tumors, *Cancer Res. 59*, 3880−3882.
11. Kreidberg, J. A. (1996) Gene targeting in kidney development, *Med. Pediatr. Oncol. 27*, 445−452.
12. Yokota, N., Nishizawa, S., Ohta, S., Date, H., Sugimura, H., Namba, H., and Maekawa, M. (2002) Role of Wnt pathway in medulloblastoma oncogenesis, *Int. J. Cancer 101*, 198−201.
13. Wagman, A. S., Johnson, K. W., and Bussiere, D. E. (2004) Discovery and development of GSK3 inhibitors for the treatment of type 2 diabetes, *Curr. Pharm. Des. 10*, 1105−1137.
14. Dominguez, I., Itoh, K., and Sokol, S. Y. (1995) Role of glycogen synthase kinase 3β as a negative regulator of dorsoventral axis formation in *Xenopus* embryos, *Proc. Natl. Acad. Sci. U.S.A. 92*, 8498−8502.
15. Rothbacher, U., Laurent, M. N., Blitz, I. L., Watabe, T., Marsh, J. L., and Cho, K. W. (1995) Functional conservation of the Wnt signaling pathway revealed by ectopic expression of *Drosophila* dishevelled in *Xenopus*, *Dev. Biol. 170*, 717−721.
16. Semenov, M. V., and Snyder, M. (1997) Human dishevelled genes constitute a DHR-containing multigene family, *Genomics 42*, 302−310.
17. Pizzuti, A., Amati, F., Calabrese, G., Mari, A., Colosimo, A., Silani, V., Giardino, L., Ratti, A., Penso, D., Calza, L., Palka, G., Scarlato, G., Novelli, G., and Dallapiccola, B. (1996) cDNA characterization and chromosomal mapping of two human homologues of the *Drosophila* dishevelled polarity gene, *Hum. Mol. Genet. 5*, 953−958.
18. Wong, H. C., Mao, J., Nguyen, J. T., Srinivas, S., Zhang, W., Liu, B., Li, L., Wu, D., and Zheng, J. (2000) Structural basis of the recognition of the dishevelled DEP domain in the Wnt signaling pathway, *Nat. Struct. Biol. 7*, 1178−1184.
19. Moon, R. T., and Shah, K. (2002) Developmental biology: Signalling polarity, *Nature 417*, 239−240.
20. Boutros, M., and Mlodzik, M. (1999) Dishevelled: At the crossroads of divergent intracellular signaling pathways, *Mech. Dev. 83*, 27−37.
21. Weston, C. R., and Davis, R. J. (2001) Signal transduction: Signaling specificity—a complex affair, *Science 292*, 2439−2440.
22. Itoh, K., Brott, B., Bae, G. U., Ratcliffe, M., and Sokol, S. (2005) Nuclear localization is required for Dishevelled function in Wnt/β-catenin signaling, *J. Biol.* (*London, U.K.*) *4* (1), 3.
23. Wong, H. C., Bourdelas, A., Krauss, A., Lee, H. J., Shao, Y., Wu, D., Mlodzik, M., Shi, D. L., and Zheng, J. (2003) Direct binding of the PDZ domain of Dishevelled to a conserved internal sequence in the C-terminal region of Frizzled, *Mol. Cell 12*, 1251−1260.
24. Cowburn, D. (1997) Peptide recognition by PTB and PDZ domains, *Curr. Opin. Struct. Biol. 7*, 835−838.
25. Umbhauer, M., Djiane, A., Goisset, C., Penzo-Mendez, A., Riou, J. F., Boucaut, J. C., and Shi, D. L. (2000) The C-terminal cytoplasmic Lys-Thr-X-X-X-Trp motif in frizzled receptors mediates Wnt/β-catenin signalling, *EMBO J. 19*, 4944−4954.
26. Wang, J., Morin, P., Wang, W., and Kollman, P. A. (2001) Use of MM-PBSA in reproducing the binding free energies to HIV-1 RT of TIBO derivatives and predicting the binding mode to HIV-1 RT of efavirenz by docking and MM-PBSA, *J. Am. Chem. Soc. 123*, 5221−5230.
27. Wang, W., Donini, O., Reyes, C. M., and Kollman, P. A. (2001) Biomolecular simulations: Recent developments in force fields, simulations of enzyme catalysis, protein−ligand, protein−protein, and protein−nucleic acid noncovalent interactions, *Annu. Rev. Biophys. Biomol. Struct. 30*, 211−243.
28. Gohlke, H., and Case, D. A. (2004) Converging free energy estimates: MM-PB(GB)SA studies on the protein−protein complex Ras-Raf, *J. Comput. Chem. 25*, 238−250.
29. London, T. B. C., Lee, H. J., Shao, Y., and Zheng, J. (2004) Interaction between the internal motif KTXXXI of Idax and mDvl PDZ domain, *Biochem. Biophys. Res. Commun. 322*, 326−332.
30. Cheyette, B. N., Waxman, J. S., Miller, J. R., Takemaru, K., Sheldahl, L. C., Khlebtsova, N., Fox, E. P., Earnest, T., and Moon, R. T. (2002) Dapper, a Dishevelled-associated antagonist of β-catenin and JNK signaling, is required for notochord formation, *Dev. Cell 2*, 449−461.
31. Gruneberg, S., Wendt, B., and Klebe, G. (2001) Subnanomolar Inhibitors from Computer Screening: A Model Study Using Human Carbonic Anhydrase II, *Angew. Chem., Int. Ed. 40*, 389−393.
32. Delaglio, F., Grzesiek, S., Vuister, G. W., Zhu, G., Pfeifer, J., and Bax, A. (1995) NMRPipe: A multidimensional spectral processing system based on UNIX pipes, *J. Biomol. NMR 6*, 277−293.
33. Goddard, T. D., and Kneller, D. G. (2000) *SPARKY 3*, University of California, San Francisco.
34. Case, D. A., Darden, T. A., Cheatham, I. T. E., Simmerling, C. L., Wang, J., Duke, R. E., Luo, R., Merz, K. M., Wang, B., Pearlman, D. A., Crowley, M., Brozell, S., Tsui, V., Gohlke, H., Mongan, J., Hornak, V., Cui, G., Beroza, P., Schafmeister, C., Caldwell, J. W., Ross, W. S., and Kollman, P. A. (2004) *AMBER 8*, Scripps Research Institute, La Jolla, CA.
35. Cornell, W. D., Cieplak, P., Bayly, C. I., Gould, I. R., Merz, K. M., Jr., Ferguson, D. M., Spellmeyer, D. C., Fox, T., Caldwell, J. W., and Kollman, P. A. (1995) A second generation force field for the simulation of proteins, nucleic acids and organic molecules, *J. Am. Chem. Soc. 117*, 5179−5197.
36. Wang, J., Wolf, R. M., Caldwell, J. W., Kollman, P. A., and Case, D. A. (2004) Development and testing of a general Amber force field, *J. Comput. Chem. 25*, 1157−1174.
37. Gohlke, H., Kiel, C., and Case, D. A. (2003) Insights into protein−protein binding by binding free energy calculation and free energy decomposition for the Ras-Raf and Ras-RalGDS complexes, *J. Mol. Biol. 330*, 891−913.
38. Kollman, P. A., Massova, I., Reyes, C., Kuhn, B., Huo, S., Chong, L., Lee, M., Lee, T., Duan, Y., Wang, W., Donini, O., Cieplak, P., Srinivasan, J., Case, D. A., and Cheatham, T. E., III (2000) Calculating structures and free energies of complex molecules: Combining molecular mechanics and continuum models, *Acc. Chem. Res. 33*, 889−897.
39. Fanning, A. S., and Anderson, J. M. (1999) Protein modules as organizers of membrane structure, *Curr. Opin. Cell Biol. 11*, 432−439.
40. Hurst, T. (1994) Flexible 3D Searching: The Directed Tweak Technique, *J. Chem. Inf. Comput. Sci. 34*, 190−196.
41. Rarey, M., Kramer, B., Lengauer, T., and Klebe, G. (1996) A fast flexible docking method using an incremental construction algorithm, *J. Mol. Biol. 261*, 470−489.
42. Clark, R. D., Strizhev, A., Leonard, J. M., Blake, J. F., and Matthew, J. B. (2002) Consensus scoring for ligand/protein interactions, *J. Mol. Graphics Modell. 20*, 281−295.
43. Zheng, J., Cahill, S. M., Lemmon, M. A., Fushman, D., Schlessinger, J., and Cowburn, D. (1996) Identification of the binding site for acidic phospholipids on the PH domain of dynamin: Implications for stimulation of GTPase activity, *J. Mol. Biol. 255*, 14−21.
44. Essmann, U., Perera, L., Berkowitz, M. L., Darden, T., Lee, H., and Pedersen, L. G. (1995) A smooth particle mesh Ewald method, *J. Chem. Phys. 103*, 8577−8593.
45. Simmerling, C., Miller, J. L., and Kollman, P. A. (1998) Combined locally enhanced sampling and particle mesh Ewald as a strategy to locate the experimental structure of a nonhelical nucleic acid, *J. Am. Chem. Soc. 120*, 7149−7155.
46. Sokol, S. Y. (1996) Analysis of Dishevelled signalling pathways during *Xenopus* development, *Curr. Biol. 6*, 1456−1467.
47. Long, J. F., Tochio, H., Wang, P., Fan, J. S., Sala, C., Niethammer, M., Sheng, M., and Zhang, M. (2003) Supramodular structure and synergistic target binding of the N-terminal tandem PDZ domains of PSD-95, *J. Mol. Biol. 327*, 203−214.
48. Feng, W., Fan, J. S., Jiang, M., Shi, Y. W., and Zhang, M. (2002) PDZ7 of glutamate receptor interacting protein binds to its target via a novel hydrophobic surface area, *J. Biol. Chem. 277*, 41140−41146.
49. Doyle, D. A., Lee, A., Lewis, J., Kim, E., Sheng, M., and MacKinnon, R. (1996) Crystal structures of a complexed and peptide-free membrane protein-binding domain: Molecular basis of peptide recognition by PDZ., *Cell 85*, 1067−1076.

BI0512602